



UNIVERSITÀ  
DEGLI STUDI  
FIRENZE

## FLORE

# Repository istituzionale dell'Università degli Studi di Firenze

### **Thermal models of dyke intrusion during development of continent-ocean transition**

Questa è la Versione finale referata (Post print/Accepted manuscript) della seguente pubblicazione:

*Original Citation:*

Thermal models of dyke intrusion during development of continent-ocean transition / Daniels, K.A.; Bastow, I.D.; Keir, D.; Sparks, R.S.J.; Menand, T.. - In: EARTH AND PLANETARY SCIENCE LETTERS. - ISSN 0012-821X. - ELETTRONICO. - 385:(2014), pp. 145-153. [10.1016/j.epsl.2013.09.018]

*Availability:*

This version is available at: 2158/1079712 since: 2020-10-28T16:23:25Z

*Published version:*

DOI: 10.1016/j.epsl.2013.09.018

*Terms of use:*

Open Access

La pubblicazione è resa disponibile sotto le norme e i termini della licenza di deposito, secondo quanto stabilito dalla Policy per l'accesso aperto dell'Università degli Studi di Firenze (<https://www.sba.unifi.it/upload/policy-oa-2016-1.pdf>)

*Publisher copyright claim:*

(Article begins on next page)



## Thermal models of dyke intrusion during development of continent–ocean transition



K.A. Daniels<sup>a,\*</sup>, I.D. Bastow<sup>b</sup>, D. Keir<sup>c</sup>, R.S.J. Sparks<sup>a</sup>, T. Menand<sup>d,e,f</sup>

<sup>a</sup> School of Earth Sciences, University of Bristol, Wills Memorial Building, Queen's Road, Bristol, BS8 1RJ, UK

<sup>b</sup> Department of Earth Science and Engineering, Imperial College London, Exhibition Road, London, SW7 2AZ, UK

<sup>c</sup> National Oceanography Centre Southampton, University of Southampton, European Way, Southampton, SO14 3ZH, UK

<sup>d</sup> Clermont Université, Université Blaise Pascal, Laboratoire Magmas et Volcans, BP 10448, F-63000, Clermont-Ferrand, France

<sup>e</sup> CNRS, UMR 6524, LMV, F-63038 Clermont-Ferrand, France

<sup>f</sup> IRD, R 163, LMV, F-63038 Clermont-Ferrand, France

### ARTICLE INFO

#### Article history:

Received 6 May 2013

Received in revised form 14 September 2013

Accepted 17 September 2013

Available online 12 November 2013

Editor: P. Shearer

#### Keywords:

dyke intrusion  
magmatic extension  
continental rifting  
heat-flow  
thermal modelling

### ABSTRACT

A consensus has emerged in recent years from a variety of geoscientific disciplines that extension during continental rifting is achieved only partly by plate stretching: dyke intrusion also plays an important role. Magma intrusion can accommodate extension at lower yield stresses than are required to extend thick, strong, unmodified continental lithosphere mechanically, thereby aiding the breakup process. Dyke intrusion is also expected to heat and thereby weaken the plate, but the spatial extent of heating and the effect of different rates of magmatic extension on the timescales over which heating occurs are poorly understood. To address this issue, a numerical solution to the heat-flow equation is developed here to quantify the thermal effects of dyke intrusion on the continental crust during rifting. The thermal models are benchmarked against a priori constraints on crustal structure and dyke intrusion episodes in Ethiopia. Finite difference models demonstrate that magmatic extension rate exerts a first-order control on the crustal thermal structure. Once dyke intrusion supersedes faulting and stretching as the principal extensional mechanism the crust will heat and weaken rapidly (less than 1 Ma).

In the Main Ethiopian Rift (MER), the majority of present-day extension is focused on ~20 km-wide Quaternary–Recent axial magmatic segments that are mostly seismogenic to mid-crustal depths and show P-wave seismic velocities characteristic of heavily intruded continental crust. When reviewed in light of our models, these observations require that no more than half of the MER's extension since ~2 Ma has been achieved by dyke intrusion. Magmatic heating and weakening of the crust would have rendered it aseismic if dyke intrusion accounted for the entire 6 mm/yr extension rate. In the older, faster extending (16 mm/yr) Red Sea rift (RSR) in Afar, dyke intrusion is expected to have had a more dramatic impact on crustal rheology. Accordingly, effective elastic plate thickness and Moho depth in the Danakil region of northernmost Afar are markedly reduced and seismicity is shallower than in the MER. Thermally driven variations in crustal rheology over time in response to dyke intrusion thus play an important role in the development of continent–ocean transition.

© 2013 The Authors. Published by Elsevier B.V. Open access under [CC BY license](#).

### 1. Introduction

It is well established that continental rifts develop initially in a mechanical fashion, with along axis segmentation governed by large-scale border faults defining early half-graben rift morphology (e.g., Hayward and Ebinger, 1996). A consensus is gradually

emerging from a number of tectonically active rifts and rifted continental margins worldwide, however, that magma intrusion also plays an important role in extension prior to the onset of sea-floor spreading (e.g., Maguire et al., 2006; White et al., 2008; Thybo and Nielsen, 2009). This is an appealing idea, since it obviates the need for large-scale tectonic forces to rupture thick, strong cratonic lithosphere: dyke intrusion can occur at lower stresses than are required for the stretching of thick continental lithosphere (e.g., Buck 2004, 2006; Bialas et al., 2010). However, the subsequent effect of magma intrusion on the thermal structure (and by inference, the strength) of the plate over time is poorly understood. It likely has important implications for the thermal evolution and subsidence history of the extending plate (e.g.,

\* Corresponding author.

E-mail addresses: [kad43@cam.ac.uk](mailto:kad43@cam.ac.uk) (K.A. Daniels), [I.Bastow@imperial.ac.uk](mailto:I.Bastow@imperial.ac.uk) (I.D. Bastow), [D.Keir@soton.ac.uk](mailto:D.Keir@soton.ac.uk) (D. Keir), [Steve.Sparks@bristol.ac.uk](mailto:Steve.Sparks@bristol.ac.uk) (R.S.J. Sparks), [T.Menand@opgc.univ-bpclermont.fr](mailto:T.Menand@opgc.univ-bpclermont.fr) (T. Menand).

<sup>1</sup> Present address: Department of Earth Sciences, University of Cambridge, Downing Street, Cambridge, CB2 3EQ, UK.

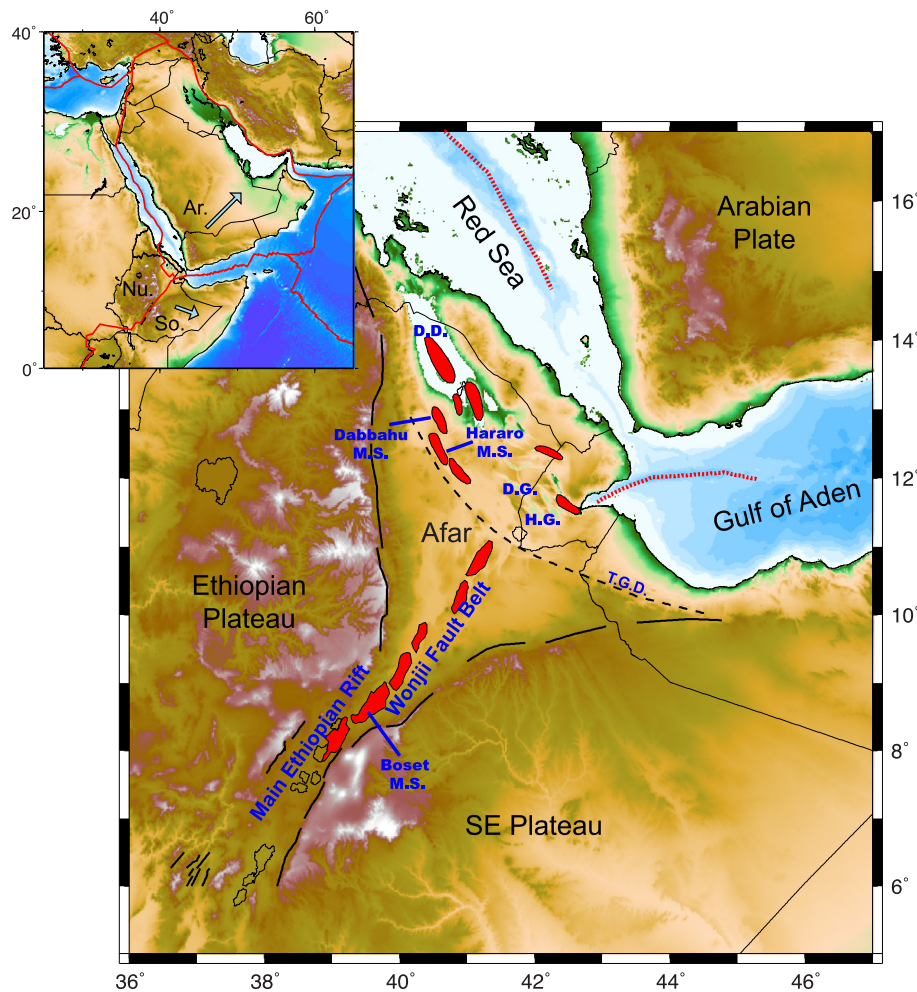


**Fig. 1.** Tectonic setting of the East African rift system in the Horn of Africa. Solid black lines show Oligocene–Miocene border faults of the Red Sea, Gulf of Aden and East African rifts. Red segments show the Quaternary–Recent sub-aerial rift axes. DD: Danakil Depression. TGD: Tendaho–Goba’ad Discontinuity. MS: magmatic segments. DG: Dobi Graben. HG: Hanli Graben. Dashed red lines are sea-floor spreading centres in the Red Sea and Gulf of Aden. Top left inset: topography of NE Africa and Arabia. Arrows show plate motions relative to a fixed Nubian plate. Red lines are plate boundaries.

Thybo and Nielsen, 2009), including whether or not continent–ocean transition is heralded by an abrupt episode of continental plate thinning and subsidence after a period of heating and weakening by protracted magma intrusion (Bastow and Keir, 2011; Keir et al., 2013).

To address these issues, a thermal model is developed to understand better the evolution of continental crust during extension by dyke intrusion. The model space is parameterised as an array of cells for which the heat-flow equation is solved numerically by finite difference scheme. The effects of variable magma temperature, dyke injection frequency and size, and geothermal gradient on the thermal evolution of the crust over time during rifting are tested by mapping the solidus and 600 °C isotherm (representing the brittle–ductile transition temperature) positions. In a tectonically active rift this is a testable hypothesis seismically, since crustal seismicity is not expected to develop at temperatures greater than ~600 °C (e.g., Maggi et al., 2000a).

To ground-truth the thermal models and input parameters, this study draws on geoscientific constraints from on-going extension in the East African (EAR) and Red Sea (RSR) rift systems in Ethiopia (Fig. 1). The region exposes sub-aerially several sections of asynchronous rift sector development above a hot (e.g., Rooney et al., 2012; Ferguson et al., 2013), low wavespeed (Bastow et al., 2008) mantle; from embryonic continental rifting in the slowly (~6 mm/yr) extending Main Ethiopian rift (MER) in the south (Kogan et al., 2012), to incipient oceanic spreading in the more

rapidly extending RSR and Gulf of Aden Rift in Afar (e.g., Hayward and Ebinger, 1996; McClusky et al., 2010). Real-time geodetic and seismic observations of dyke intrusion episodes (Wright et al., 2006; Keir et al., 2009; Grandin et al., 2011) are available from the region, offering considerable advantage over studies of extinct or buried rifted margins in constraining when and how dykes intrude the crust. The region is also well-understood geophysically, with detailed constraints on parameters such as crustal thickness, effective elastic plate thickness and P-wave seismic velocity structure all available (for reviews, see e.g., Bastow et al., 2011; Keir et al., 2013).

In the MER, a combination of GPS surveys and structural geology studies point towards ~80% of present-day strain being accommodated at least partly by magma intrusion within a relatively narrow (~20 km) rift-axial zone, also known as the Wonji Fault Belt (WFB: Mohr, 1967; Ebinger and Casey, 2001). However, precisely what proportion of extension has been accommodated by dyke intrusion into the still-thick MER crust since ~2 Ma is uncertain. In the Danakil depression, where crustal thickness is markedly thinner than elsewhere in Afar (Makris and Ginzburg, 1987), it has been proposed that Pliocene–Recent basin development and voluminous Quaternary volcanism are the result of a late-stage of plate stretching following a protracted period of localised magma-intrusion (Bastow and Keir, 2011; Keir et al., 2013). This study explores whether episodes of dyke intrusion during continental breakup are capable of heating the continental crust sufficiently

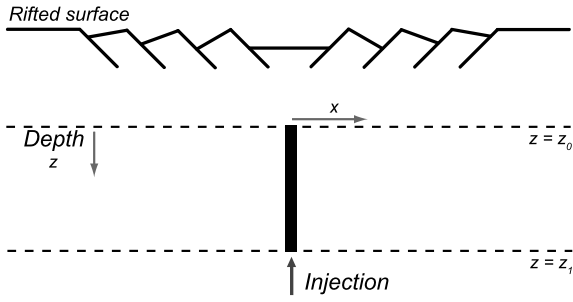


**Fig. 2.** A schematic diagram showing the set-up of the model relative to the overlying rift topography, and the dimensions and position of the computational domain within the crust.

over time for it then to behave in a ductile manner by plate stretching, prior to the development of a new mid-ocean spreading centre.

## 2. Mathematical model

The thermal evolution of a vertical dyke intruded into continental crust (Fig. 2) is modelled by solving the two-dimensional (2D) heat-flow equation both horizontally ( $x$ -direction) and in depth ( $z$ ). The model is set-up in a similar manner to previous studies (Royden et al., 1980; Buck, 2004; Buck et al., 2005; Bialas et al., 2010) with a vertical cross-section through the crust incorporating a model rift axis where consecutive dykes intrude along the centre of the previous one. The dykes are intruded at a time-averaged rate which is constant at all depths ( $z$ ) beneath the rift axis. Homogeneous composition continental crust is assumed, such that thermal conductivity ( $K$ ), diffusivity ( $\kappa$ ), density ( $\rho$ ), specific heat capacity ( $C_p$ ) and latent heat of fusion ( $L$ ) remain constant as a function of depth and temperature. The 2D heat-flow equation, incorporating the latent heat of fusion is

$$\rho C_p \frac{\partial T}{\partial \tau} + \rho L \frac{\partial X}{\partial \tau} = K \nabla^2 T \quad (1)$$

where  $\nabla^2 = \frac{\partial^2}{\partial x^2} + \frac{\partial^2}{\partial z^2}$ ,  $T(x, z, \tau)$  is the temperature,  $X(x, z, \tau)$  is the melt fraction and  $\tau$  is the time (e.g., Turcotte and Schubert, 2002). Melt fraction is assumed to depend only on temperature such that

$$X = F(T) \quad (2)$$

where  $F$  is a function derived from a simple three-component phase diagram based on a Hawaiian olivine tholeiite basalt (Sample 14, Yoder and Tilley, 1962) with three components; the chemical analysis was recalculated as a CIPW norm (Cox et al., 1979) and the components were re-normalised to give olivine, clinopyroxene and plagioclase. The melt fractions corresponding to temperatures in the range 0 to 1320 °C were calculated using the simulated phase equilibria model of Witham (2008). The simple three-phase system was used to test the model's performance when compared with analytical solutions, and to explore the effects of different parameters.  $F$  (Eq. (2)) is generally determined from experimental studies. Here, it is approximated by a series of linear trends.

The far-field geotherm  $T(z)$  is assumed to satisfy the boundary conditions

$$T \rightarrow \frac{Q_0}{K}z - \frac{A}{2K}z^2 \quad \text{as } x \rightarrow \pm\infty \quad (3)$$

where the surface temperature is taken to be zero. This equation is valid for all values of  $z$ . The initial condition for a single injection is

$$T = T_m, \quad |x| < \omega; \\ T = \frac{Q_0}{K}z - \frac{A}{2K}z^2, \quad |x| > \omega \quad \text{at } \tau = 0 \quad (4)$$

for  $z_0 \leq z \leq z_1$ , where  $z_0$  and  $z_1$  define the upper and lower surfaces of the modelled region of the crust (Fig. 2) and whose temperature satisfies Eq. (3) such that  $T = \frac{Q_0}{K}z_0$  at  $z = z_0$  and  $T = \frac{Q_0}{K}z_1$  at  $z = z_1$ ,  $T_m$  is the magma injection temperature at time  $\tau = 0$  and  $2\omega$  is the dyke width. Above and below the intruded region ( $z < z_0$  and  $z > z_1$ ), the thermal evolution of the crust is governed by the geotherm (Eq. (3)). Solutions of Eqs. (1)–(4) are required to determine how the temperature and melt fraction evolve as functions of  $x$ ,  $z$ , and  $\tau$ . Numerical solutions of Eqs. (1)–(4) were determined using an explicit finite difference method. A full description of the finite difference method is included as Appendix A.

The heat-flow equation (Eq. (1)) was discretised using forward difference approximations in  $\tau$  and a central difference approximation in  $x$ . The solution was computed forwards in time by incrementing the timestep ( $k$ ) through integer values, starting with  $k = 0$  where  $T$  and  $X$  are determined by the initial temperature profile (Eq. (6)). Due to the symmetrical nature of the solution about  $x = 0$ , the computational domain was restricted to positive  $x$  values and a symmetry condition applied to the left hand edge of the domain. Successive intrusions of basalt at a constant injection rate were modelled numerically by displacing previously computed values of temperature rightwards (mimicking advection) by the half-dyke width at each new injection time and inserting the new intrusion of the same dyke width and temperature  $T_m$  in the space vacated. The advection of heat due to ductile stretching of the crust is not considered in our models since it will be negligible over the timescales we model intrusions. Brittle deformation by faulting has also not been accounted for in the model. The injection frequency  $\psi$  was defined as the ratio of the magmatic extension rate  $S$  to the dyke thickness  $2\omega$  so that  $S = 2\omega\psi$ .

## 3. Specific model parameterisation for Ethiopia

The tectonically active East African Rift (EAR) and southern Red Sea Rift (RSR) in Ethiopia provide an excellent opportunity to source realistic input parameters for our thermal model (Fig. 1). The starting composition was established using the lava from a 2007 fissure eruption in Afar (sample A2, Ferguson et al., 2010), with a water content of 0.4 wt% assumed at all depths. The series of linear fits used for the temperature–melt fraction relationship were determined using the MELTS (Ghiorso and Sack, 1995; Asimow and Ghiorso, 1998) and Rhyolite-MELTS (Gualda et al., 2012) thermodynamic modelling programs. The composition of the injected material and the intruded crust are assumed to be the same. Because the injected material mainly cools and the host rock predominantly slowly increases in temperature, the temperature–melt fraction relationship of the host material is not important and will not affect the temperatures produced (Daniels, 2012). The solidus temperature was based on previously published model temperatures (Annen and Sparks, 2002).

The temperature–melt fraction relationship was calculated for four different pressures corresponding to different depths in the crust:  $z = 5, 10, 15$  and  $20$  km (Fig. 3). It has been inferred from wide-angle seismic (Maguire et al., 2006), gravity (Cornwell et al., 2006) and electrical resistivity (Desissa et al., 2013) study in Ethiopia that gabbroic intrusions occur in this depth range in the upper crust beneath Quaternary–Recent zones of magmatic extension. Partial melt is also known to reside at these depths, as revealed by magnetotelluric analysis of the subsurface (Whaler and Hautot, 2006). The lithostatic pressures and corresponding depths (calculated using  $\rho gh$  with  $\rho = 2800$  kg/m<sup>3</sup>, Annen and Sparks, 2002), along with all of the crystallisation points, are in Table 1. Values of the physical parameters assumed are summarised in Table 2. A dyke thickness of 15 m allowed different extension rates  $S$  to be achieved by varying the dyke injection frequency  $\psi$ . Previous

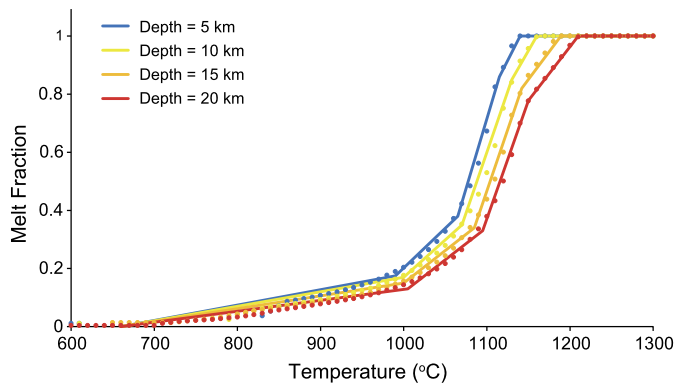


**Fig. 3.** Temperature versus melt fraction for 4 different pressures, calculated using MELTS (Ghiorso and Sack, 1995; Asimow and Ghiorso, 1998), Rhyolite-MELTS (Gualda et al., 2012) and experimental estimates of the water-saturated granite solidus (Stern and Wyllie, 1973; Annen and Sparks, 2002). Small differences in the melt fraction–temperature relationship will have a minimal effect on the results.

**Table 1**

Temperatures ( $T$ ) in °C, and corresponding melt fractions ( $X$ ) for four different pressures: 137.34 MPa (5 km depth); 274.68 MPa (10 km depth); 412.02 MPa (15 km depth); and 549.36 MPa (20 km depth). Subscripts  $l$ ,  $e$  and  $s$  correspond to the liquidus, eutectic and solidus temperatures respectively;  $c$  and  $c2$  are arbitrary points on the  $X$ – $T$  diagram chosen to give the best fit to the data.

| Pressure | 1373.4 | 2746.8 | 4120.4 | 5493.6 |
|----------|--------|--------|--------|--------|
| $T_l$    | 1140   | 1160   | 1189   | 1210   |
| $X_l$    | 1      | 1      | 1      | 1      |
| $T_c$    | 1115   | 1130   | 1142   | 1150   |
| $X_c$    | 0.860  | 0.850  | 0.820  | 0.778  |
| $T_{c2}$ | 1065   | 1070   | 1085   | 1095   |
| $X_{c2}$ | 0.380  | 0.350  | 0.340  | 0.330  |
| $T_e$    | 990    | 1000   | 1000   | 1005   |
| $X_e$    | 0.175  | 0.170  | 0.150  | 0.130  |
| $T_s$    | 660    | 660    | 660    | 660    |
| $X_s$    | 0      | 0      | 0      | 0      |

**Table 2**

Nomenclature – model parameters and input values.

| Parameter            |                                     | Values               | Units             |
|----------------------|-------------------------------------|----------------------|-------------------|
| $\Delta x, \Delta z$ | Array cell size                     | 5                    | m                 |
| $\Delta t$           | Timestep size                       | 3 110 400            | s                 |
| $\omega$             | Dyke half thickness                 | 15                   | m                 |
| $\rho$               | Density <sup>a</sup>                | 2800                 | kg/m <sup>3</sup> |
| $k$                  | Thermal conductivity <sup>b</sup>   | 2.2                  | W/m/K             |
| $\kappa$             | Thermal diffusivity                 | $5.3 \times 10^{-7}$ | m <sup>2</sup> /s |
| $L$                  | Specific latent heat <sup>a</sup>   | $4 \times 10^5$      | J/kg/K            |
| $C_p$                | Specific heat capacity <sup>a</sup> | 1480                 | J/kg              |
| $Q_o$                | Surface heat flux <sup>c</sup>      | 60                   | mW/m <sup>2</sup> |
| $A$                  | Heat production <sup>c</sup>        | $8 \times 10^{-7}$   | W/m <sup>3</sup>  |

<sup>a</sup> Annen and Sparks (2002).

<sup>b</sup> Jaupart and Mareschal (2007).

<sup>c</sup> Jaupart and Mareschal (2011).

models that varied dyke thickness and injection frequency whilst fixing extension rate have shown that thinner, more frequently intruded dykes increase the crustal temperature more quickly than thicker, less frequently intruded dykes, but the effect is insignificant compared with other parameters such as the extension rate (Daniels, 2012). It is for this reason that only one dyke thickness is chosen. Injection temperatures ( $T_m$ ) in the range 1240–1320 °C were studied.

#### 4. Results

Two-dimensional model runs with  $x_0 = 0$ ,  $x_1 = 10$  km,  $z_0 = 0$ ,  $z_1 = 10$  km,  $\Delta x = \Delta z = 5$  m and dyke width = 15 m were con-

**Table 3**

Time taken in years for the temperature at the injection line,  $x = 0$ , to reach the solidus temperature and the 600 °C isotherm for different extension rates and depths.

|                 | Extension rate (mm/yr) | Depth (km)         |                    |                    |                    |
|-----------------|------------------------|--------------------|--------------------|--------------------|--------------------|
|                 |                        | 5                  | 10                 | 15                 | 20                 |
| Solidus         | 3                      | $1.18 \times 10^6$ | $8.18 \times 10^5$ | $4.63 \times 10^5$ | $2.17 \times 10^5$ |
|                 | 5                      | $3.96 \times 10^5$ | $2.66 \times 10^5$ | $1.66 \times 10^5$ | $8.29 \times 10^4$ |
|                 | 10                     | $1.01 \times 10^5$ | $6.96 \times 10^4$ | $4.30 \times 10^4$ | $2.23 \times 10^4$ |
|                 | 20                     | $2.60 \times 10^4$ | $1.79 \times 10^4$ | $1.12 \times 10^4$ | $6.06 \times 10^3$ |
|                 | 25                     | $1.67 \times 10^4$ | $1.14 \times 10^4$ | $7.24 \times 10^3$ | $3.70 \times 10^3$ |
| 600 °C isotherm | 3                      | $8.18 \times 10^5$ | $5.18 \times 10^5$ | $2.91 \times 10^5$ | $1.04 \times 10^5$ |
|                 | 5                      | $3.04 \times 10^5$ | $1.92 \times 10^5$ | $1.04 \times 10^5$ | $3.86 \times 10^4$ |
|                 | 10                     | $7.82 \times 10^4$ | $5.04 \times 10^4$ | $2.81 \times 10^4$ | $1.05 \times 10^4$ |
|                 | 20                     | $2.01 \times 10^4$ | $1.35 \times 10^4$ | $7.39 \times 10^3$ | $2.96 \times 10^3$ |
|                 | 25                     | $1.32 \times 10^4$ | $8.43 \times 10^3$ | $4.88 \times 10^3$ | $1.92 \times 10^3$ |

ducted for extension rates of 5, 10, 15 and 20 mm/yr and for a duration of 200 ka. In these models, the injected dyke extended over the depth of the computational array. Fig. 4 shows the output of these 2D models and the brittle–ductile transition (black line) and solidus (red line) isotherms migrating across the computational domain. Loss of heat at the top and bottom of the domain can be seen to affect the temperatures.

As detailed in the supplementary material, the model was tested successfully against independent analytical solutions. Moreover, except at the top and bottom of the model, this 2D numerical model can be approximated by a 1D model where the temperature profile depends only on the horizontal distance  $x$  at a given, constant depth  $z$ : both 1D and 2D numerical models yield similar solutions (see the supplementary material for details). However, at the top and bottom of the modelled region of the crust, the thermal boundary conditions influence the solution there immediately and eventually affect the solution throughout the model space. But, if these upper and lower boundaries ( $z_0$  and  $z_1$ ) are sufficiently far apart, the 1D model yields a very good approximation for the model interior, thus reducing computational time considerably.

At the top of the 2D model, the boundary effect is analogous to the surface cooling of the system (see the supplementary material for details). The amount of the modelled crust affected after time  $\tau$  can be approximated using  $l^2 \sim \kappa \tau$  such that after 1 Ma, the top 4 km of the crust will have experienced surface cooling, increasing to 7 km after 3 Ma. For depths  $>5$  km, the 1D heat-flow equation is thus appropriate for the study of the thermal structure of continental crust during extension by dyke intrusion over a time period of a couple of Ma.

The 1D numerical model was run using the parameters in Table 2 for extension rates of 3, 5, 10, 20, and 25 mm/yr, for a horizontal range of  $x_0 = 0$  to  $x_1 = 30$  km and at depths ( $z$ ) of 5, 10, 15, and 20 km. These extension rates were designed to encompass the  $\sim 6$  mm/yr extending MER, and the  $\sim 16.4$  mm/yr extending RSR in Afar. Each model was run for 5 Ma, with temperature monitored as a function of distance from the dyke injection point. Particular attention was paid to the solidus temperature and brittle–ductile transition (600 °C) isotherms. Magmatic extension rate and the time taken to reach the solidus temperature or the brittle–ductile 600 °C isotherm at the injection position ( $x = 0$ ) display an inverse power law relationship ( $S$  is proportional to  $\frac{1}{\sqrt{t}}$ ; Figs. 5 and 6). Thus, magmatic extension rate is approximately proportional to  $\frac{1}{\sqrt{t}}$ , independent of injection temperatures (Fig. 5). Injection temperature is thus secondary to extension rate in governing the rate of temperature increase.

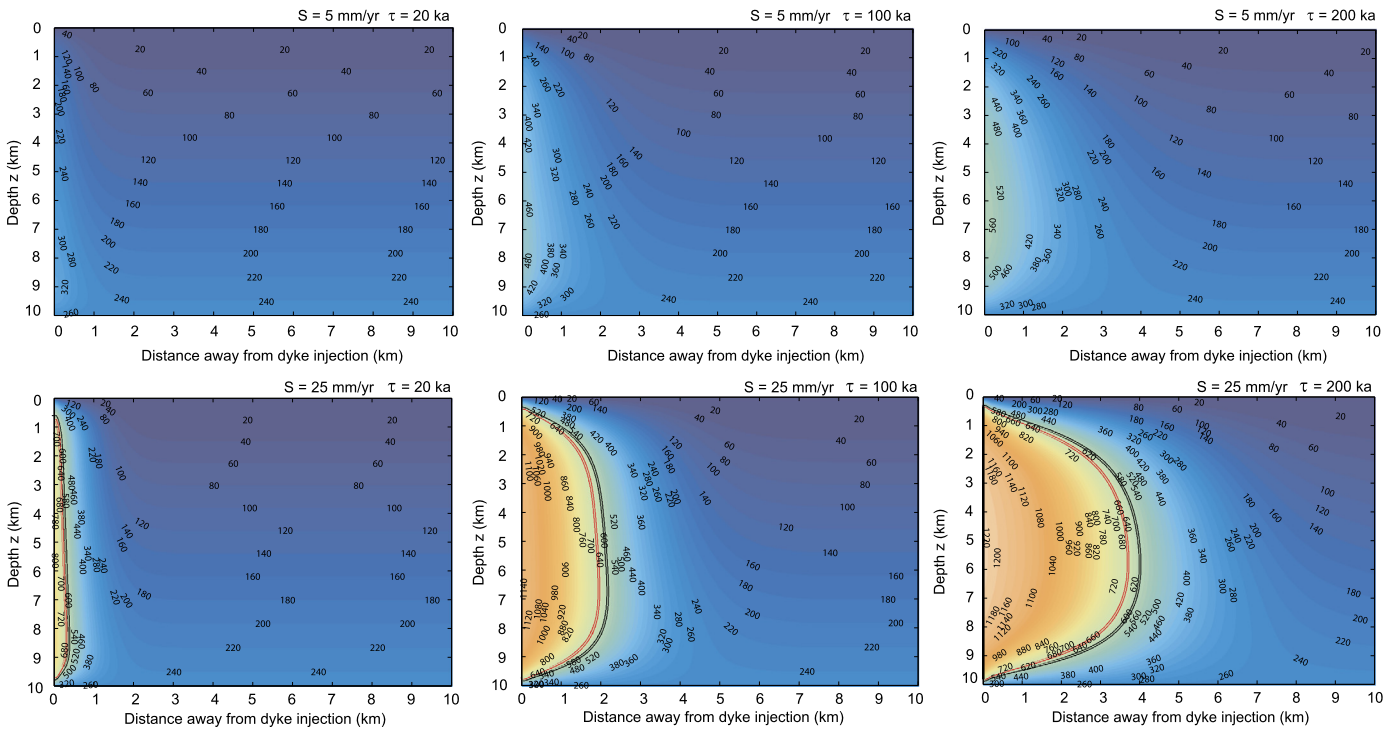


**Fig. 4.** Outputs from two-dimensional model runs with  $z_0 = 0$  and  $z_1 = 10$  km, and  $\tau = 20$  ka, 100 ka and 200 ka. Above: extension rate  $S = 5$  mm/yr. Below:  $S = 20$  mm/yr. The brittle-ductile transition (black line) and solidus (red line) isotherms are highlighted.

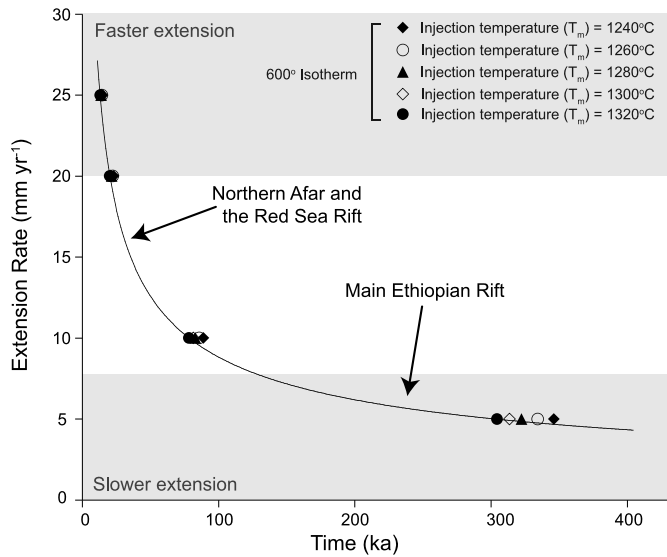


**Fig. 5.** Extension rate versus the time, expressed in ka, taken to reach the 600°C isotherm temperature at 5 km depth at the injection position. The extension rates of the MER (~6 mm/yr) and RSR (15–20 mm/yr) are highlighted. The injection temperatures are in the range  $T_m = 1240$  to 1320°C.

The distance ( $x$ ) from the dyke injection and the time taken to reach a given isotherm correlate linearly for all extension rates ( $S$ ) (Fig. 7A). The linear trend indicates that the magmatic extension rate is dominant at distances close to the dyke injection location. Fig. 7B shows modelled isotherm positions as a function of distance from the dyke injection point; also shown are isotherm positions determined from extension rate alone (effects of conduction are close to negligible). Extension rate is a good proxy for isotherm migration rate in the near field, but with increasing distance from the injection point, conduction becomes an increasingly important additional effect.

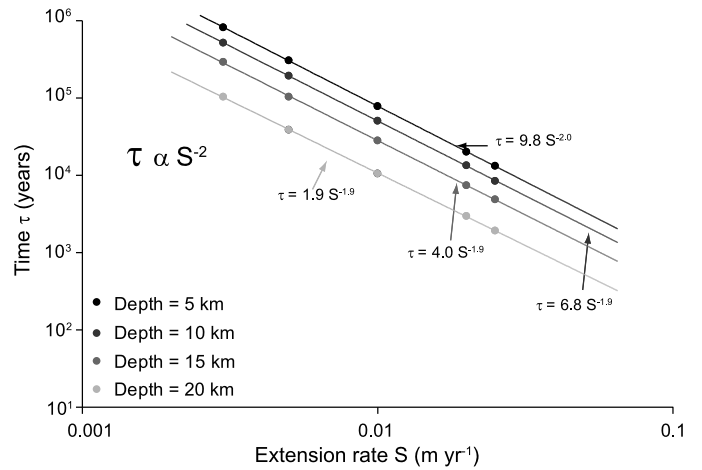


**Fig. 6.** Time taken to reach the 600°C isotherm temperature as a function of extension rate.

When the time is plotted as a function of extension rate (Fig. 6), the results are comparable with the results of Michaut and Jaupart (2006) who found that the critical temperature in their numerical models ( $t_c$ ) was inversely proportional to injection rate squared ( $Q^2$ ). The constant that multiplies the injection rate in each of the relationships in Fig. 6 is dependent on the parameters used in the modelling (Table 2) and therefore is different for each case. However, in both this study and in Michaut and Jaupart (2006), the time taken to reach a particular temperature is inversely proportional to the square of the extension rate. The timescales for the build up of temperature calculated for different magmatic extension rates are quite varied. Calculations show that it will take significantly longer for the ambient temperature to build up at slower extension rates: an extension rate three times faster will decrease this time by an order of magnitude (Fig. 5).

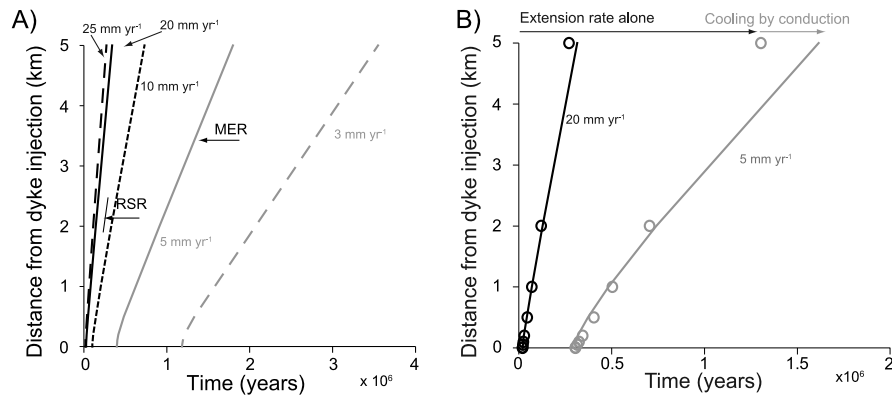


**Fig. 7.** (A) Time taken to reach the solidus temperature as a function of the distance away from the dyke injection point, at 5 km depth. (B) The position of the 600 °C isotherm (solid lines and unfilled dots) due to the model (lines) and the extension rate alone (dots). The component of the extension rate alone is calculated using the time taken to reach the 600 °C isotherm at distance  $x = 0$  as the starting point, and then migrating the isotherm away from the starting point at the magmatic extension rate. Extension rates of 5 mm/yr (grey solid lines and unfilled dots) and 20 mm/yr (black solid lines and unfilled dots) are shown. The arrows show the components of extension alone (black arrow) versus the cooling due to conduction (grey arrow). The first arrow is much longer than the second one, illustrating that the time taken to reach the isotherm is primarily controlled by the extension rate; accounting for heat loss by conduction increases this time but this effect appears to be secondary.

## 5. Discussion

### 5.1. Overview

It is now well established that dyke intrusion achieves a significant proportion of extension during continental rifting (e.g., Maguire et al., 2006; Thybo and Nielsen, 2009; White et al., 2008), yet relatively little attention has been paid in the rifting community to the effects this has on the thermal evolution (and by inference the strength) of the continental crust during breakup. Previous studies have demonstrated that appreciable crustal heating occurs due to repeated magma intrusion in arc settings (e.g. Annen et al., 2006; Solano et al., 2012), and a similar thermal modelling approach has been followed in this study of continental rifting.

This study demonstrates that the thermal structure of the crust is controlled by several factors: intrusion depth, injection temperature, and magmatic extension rate. Of these, magmatic extension rate exerts first-order control on crustal thermal structure (Figs. 5, 6 and 7). The rate of transfer of heat laterally away from the zone of dyke intrusion can be approximated in the near-field by the magmatic extension rate, but at greater distances (>3–4 km), cooling by conduction becomes an important factor (Fig. 7).

The location of the injection relative to the previous injection is also likely play a role in the timescale of the build up of heat in the crust. Here, each successive injection has intruded through the centre of the previous injection. This may have had the effect of insulating each hot injection from the cooler crust to either side and therefore indicate that the timescales calculated represent minimum estimates. Additionally, the advection of heat due to ductile stretching of the crust has not been accounted for in the model. At slow extension rates relevant for continental rift zones, this effect is negligible compared to the marked and rapid heating caused by intrusion. At faster rates of extension observed at mid-ocean ridges, but rare for continental rifts, the advection of heat is likely more important.

Observations of seismicity worldwide indicate strongly that earthquake depths are fundamentally limited by the brittle–ductile transition in continental crust and commonly the 600 °C isotherm is used to mark this transition in typical crust (e.g., Maggi et al., 2000a, 2000b; Jackson, 2002). A 10–20 km wide region of the crust would be expected to heat to above 600 °C in <1 Ma, even at relatively slow extension rates of ~10 mm/yr (Fig. 7). At slower rates, heating to 600 °C will take much longer (e.g., 6.3 Ma for a 20 km-wide region at 3 mm/yr).

### 5.2. Implications for the thermal development of the MER

The MER is the northern-most sector of the EAR and displays several stages of rift sector development along strike. Embryonic continental rifting in the southern MER is dominated by border faulting while in the northern MER, rifting is more evolved and axial magma intrusion contributes significantly to Nubia–Somalia separation (e.g., Hayward and Ebinger, 1996; Kogan et al., 2012). The northern MER has also undergone considerable development over time: initial rifting during Miocene times was characterised by upper-crustal extension accommodated by the large-offset border faults that define the rift valley flanks today (e.g., Wolfenden et al., 2005). Since Quaternary times however, faulting and volcanism have localised to the 20–30 km wide WFB axial zone. Aligned Quaternary–Recent monogenetic basaltic cones and resultant lava flows cut by the most active faults within the MER, coupled with geodetic evidence that ~80% of Nubia–Somalia plate separation is presently accommodated within the WFB (Bilham et al., 1999), was cited by Ebinger and Casey (2001) as evidence that a significant proportion of extension in the MER is achieved by episodic magma intrusion. More recent studies of GPS measurements acquired over the last two decades confirm the MER is currently opening at 5–6 mm/yr in an ESE–WNW direction (Kogan et al., 2012). The seismic moment release in the MER since 1960 is around half that expected from the plate separation velocities, which suggests 50% of the extension is accommodated by aseismic processes such as magma intrusion (Hofstetter and Beyth, 2003).

The 2001–2003 Ethiopia Afar Geoscientific Lithospheric Experiment (see Bastow et al., 2011 for a review) has facilitated the development of high-resolution subsurface geophysical models of the MER. Wide-angle active-source, passive-seismic, and gravity studies of crustal structure have shown that zones of Quaternary–Recent magmatism in the WFB are underlain by anomalously high P-wavespeed and high-density material compared to surrounding native continental crust (e.g., Keranen et al., 2004; Mackenzie et al., 2005; Daly et al., 2008; Cornwell et al., 2006; Maguire et al., 2006; Tiberi et al., 2005). These are interpreted as zones of localised gabbroic intrusions that extend from the aligned monogenetic cone fields along the rift axis surface to the base of the crust at 30–35 km depth (e.g., Keranen et al., 2004; Mackenzie et al., 2005). While the total volume of new intruded material beneath the axis is debated, the marked reduction in seismic velocities in the upper ~8 km of the crust suggests intrusion contributes a lower proportion of extension at these shallow depths compared to elsewhere in the crust (Keranen et al., 2004).

The thermal models developed in this study show that  $\sim 6$  mm/yr extension in the MER should, if achieved 100% by magma intrusion, by now have heated the crust to temperatures in excess of 600 °C (Figs. 5 and 7). Observations of seismicity in the MER render this hypothesis implausible, however. Variations in seismicity along the WFB instead demonstrate along-axis variability in the thermal state of the crust. The Boset segment (Fig. 1) is the most magmatically active portion of the MER (e.g. Abebe et al., 2007) and accordingly exhibits the least seismicity and shallowest brittle–ductile transition at 6–9 km depth (Beutel et al., 2010). Crustal tomographic studies indicate the highest P-wavespeed anomalies anywhere along the MER occur in the Boset segment, with the implication that the crust here contains a higher proportion of new igneous material than elsewhere along the rift (e.g. Keranen et al., 2004; Maguire et al., 2006). In other areas of the MER, with lower amplitude high P-wavespeed anomalies, seismicity is evident to depths of 15–18 km, indicating higher crustal strength and lower temperatures (Beutel et al., 2010).

If only 50% of the 6 mm/yr extension in the MER has been achieved by dyke intrusion beneath the WFB, the thermal models presented in this study would predict a significantly smaller degree of heating and weakening. Extrapolating from Fig. 7, a zone 20 km wide would heat to the brittle–ductile transition at all depths only after about 6 Ma. This is a longer period of time than the WFB has existed within the MER: earlier extension was confined to the large-offset border faults (Wolfenden et al., 2005). The depth extent of seismicity and variations in P-wave speeds beneath the magmatic segment along the axis of the MER when interpreted in light of our thermal modelling supports the interpretation that the crust beneath the WFB is not 100% new mafic material. Rather it is a zone of heavily intruded continental crust. Mechanical extension (faulting and stretching) thus remains an important mechanism of strain accumulation between Nubia and Somalia.

### 5.3. Implications for the development of continent–ocean transition

In contrast to the relatively young magmatic phase of extension observed in the MER, Afar has experienced magma-assisted rifting since the Miocene (Wolfenden et al., 2005). Our models predict that given the higher extension rate ( $\sim 16$  mm/yr) and longer period of time elapsed since the onset of magma intrusion, crustal temperatures should be too high for brittle deformation to occur; the crust should thus now be able to deform in a ductile manner (stretching). However, most of sub-aerial Afar has generally thick crust (Makris and Ginzburg, 1987; Hammond et al., 2011), and is still seismically active (Ayele et al., 2007a, 2007b; Keir et al., 2011a, 2011b; Ebinger et al., 2013) indicating that magma intrusion has not thermally weakened the plate as much as suggested by the model. A simple explanation for this is that the Arabia–Nubia plate boundary has shifted north-eastward several times in response to triple junction development in Afar. During earlier phases of magma-assisted rifting in Miocene times, strain was accommodated in magmatic segments located proximal to the western southern Red Sea border fault on the western margin of Afar (e.g. Wolfenden et al., 2005). Since then, strain has localised progressively north-eastward to form the current configuration of axial volcanic segments (e.g. Dabbahu and Hararo segments) and sometimes amagmatic grabens (e.g. Tendaho; Dobi and Hanle graben: Tesfaye et al., 2003). Consequently, magma intrusion is unlikely to have been localised for long enough in any given location for sufficient crustal heating to occur. As a result, extension by dyke intrusion remains the optimal straining mechanism (e.g., Buck, 2006), with plate strength likely still too high to permit significant ductile stretching localised around the intrusion zone.

Our thermal models show that only when dyke intrusion is focused to one magmatic segment for a protracted period of time would aseismic ductile deformation be expected to commence (Figs. 5 and 7). One region where this transition may be underway is the sub-aerial but below sea-level Danakil depression in northernmost Afar. Here rapid basin subsidence since  $\sim 5$  Ma indicated by 3–5 km accumulations of Pliocene–Recent sediments, combined with a pulse of Quaternary–Recent fissural basaltic volcanism, were interpreted by Bastow and Keir (2011) as evidence for a late stage of plate stretching and an increase in decompression melting in the mantle. The Bastow and Keir (2011) study lacked constraint on the mechanism responsible for the shift from extension by magma intrusion to extension by ductile stretching, but noted that late-stage subsidence and volcanism is a common feature of the geological record at magmatic rifted margins globally. The thermal models presented in this study show that at the  $\sim 10$  mm/yr extension rates observed in the Danakil depression (McClusky et al., 2010), a 20 km wide zone will be sufficiently heated at 5 km depth after about 1 Ma of extension by magma intrusion to deform in a ductile fashion (Fig. 7). However, in the Danakil depression where plate stretching has commenced, heat advection is likely to be a considerable additional component. A hotter and weaker plate in the Danakil depression is supported by earthquakes restricted to the upper  $\sim 5$  km of the crust (e.g., Craig et al., 2011; Nobile et al., 2012), and  $\sim 5$  km effective elastic plate thickness derived from gravity–topography coherence studies of plate strength (Ebinger and Hayward, 1996; Pérez-Gussinyé et al., 2009). When synthesised in light of a priori geoscientific constraints from the Danakil region, our thermal models thus indicate that a late-stage of localised plate stretching, with an associated pulse of decompression melting, can readily characterise the final stages of continent to ocean transition.

## 6. Conclusions

We have developed a numerical solution to the heat-flow equation to quantify the effects of dyke intrusion on the thermal structure of the crust during rifting, and on the timescales of the heating at varying magmatic extension rates. The rate of extension by intrusion is shown to exert first-order control on crustal thermal structure, and when extension is achieved entirely by dyke intrusion, the crust is expected to heat considerably on timescales of less than 1 Ma.

We benchmarked our thermal models against recently developed constraints on crustal structure and dyke intrusion episodes in Ethiopia. For the MER, our model predicts brittle deformation at the ultra-slow extension rates of  $\sim 6$  mm/yr will cease after only 300 ka of entirely magmatic extension localised to the rift axis. Our thermal calculations, corroborated by observations of seismic moment release, depth extent of seismicity, and P-wave speeds, point instead to a rifting model by which only  $\sim 50\%$  of the extension is accommodated by magma intrusion. In the Danakil depression of northernmost Afar in contrast, a combination of faster extension rates of  $\sim 10$  mm/yr and longer history of magma intrusion has likely resulted in sufficient heating and weakening of the plate to induce a late stage phase of localised ductile stretching near the intruded zone. Our results demonstrate the significant impact of dyke intrusion on the rheology of continental crust during rifting. The challenge now is to understand better how dyke intrusion affected plate strength during the development of magmatic margins worldwide.

## Acknowledgements

K.A.D. would like to thank G.P. Daniels, P.G. Daniels and F. Witham for early assistance with the numerical coding and help-



ful discussions thereafter. C. Annen, J.D. Blundy, G.A. Jones and K.A. Whaler are also thanked for constructive comments and suggestions. The authors are grateful to three anonymous reviewers whose comments have strengthened and improved the manuscript. K.A.D. was supported by a NERC Consortium Grant. R.S.J.S. is co-supported by a grant from the European Research Council who also provided the funding for the manuscript's colour figures. I.D.B. is funded by the Leverhulme trust. This is Laboratory of Excellence *ClerVolc* contribution no. 77.

## Appendix A. Supplementary material

Supplementary material related to this article can be found online at <http://dx.doi.org/10.1016/j.epsl.2013.09.018>.

## References

- Abebe, B., Acocella, V., Kome, T., Ayalew, D., 2007. Quaternary faulting and volcanism in the Main Ethiopian Rift. *J. Afr. Earth Sci.* 48, 115–124.
- Annen, C., Sparks, R.S.J., 2002. Effects of repetitive emplacement of basaltic intrusions on thermal evolution and melt generation in the crust. *Earth Planet. Sci. Lett.* 203, 937–955.
- Annen, C., Blundy, J.D., Sparks, R.S.J., 2006. The genesis of intermediate and silicic magmas in deep crustal hot zones. *J. Petrol.* 47 (3), 505–539.
- Asimow, P.D., Ghiorso, M.S., 1998. Algorithmic modifications extending MELTS to calculate subsolidus phase relations. *Am. Mineral.* 83, 1127–1131.
- Ayele, A., Stuart, G., Bastow, I., Keir, D., 2007a. The August 2002 earthquake sequence in north Afar: Insights into the neotectonics of the Danakil microplate. *J. Afr. Earth Sci.* 48 (2), 70–79.
- Ayele, A., Jacques, E., Kassim, M., Kidane, T., Omar, A., Tait, S., Necessian, A., deChabalier, J.-B., King, G., 2007b. The volcano-seismic crisis in Afar, Ethiopia, starting September 2005. *Earth Planet. Sci. Lett.* 255, 177–187.
- Bastow, I.D., Keir, D., 2011. The protracted development of the continent ocean transition in Afar. *Nat. Geosci.* 4, 248–250.
- Bastow, I.D., Nyblade, A.A., Stuart, G.W., Rooney, T., Benoit, M.H., 2008. Upper mantle seismic structure beneath the Ethiopian hotspot: rifting at the edge of the African low velocity anomaly. *Geochem. Geophys. Geosyst.* 9 (12). <http://dx.doi.org/10.1029/2008GC002107>.
- Bastow, I.D., Keir, D., Daly, E., 2011. The Ethiopia Afar Geoscientific Lithospheric Experiment (EAGLE): Probing the transition from continental rifting to incipient seafloor spreading. In: Beccaluva, L., Bianchini, G., Wilson, M. (Eds.), *Volcanism and Evolution of the African Lithosphere*. In: *Spec. Pap., Geol. Soc. Am.*, vol. 478, pp. 51–76.
- Beutel, E., van Wijk, J., Ebinger, C., Keir, D., Agostini, A., 2010. Formation and stability of magmatic segments in the Main Ethiopian and Afar rifts. *Earth Planet. Sci. Lett.* 293, 225–235.
- Bialas, R.W., Buck, W.R., Qin, R., 2010. How much magma is required to rift a continent? *Earth Planet. Sci. Lett.* 292, 68–78.
- Bilham, R., Bendick, R., Larson, K., Mohr, P., Braun, J., Tesfaye, S., Asfaw, L., 1999. Secular and tidal strain across the main Ethiopian rift. *Geophys. Res. Lett.* 26 (18), 2789–2792.
- Bohrson, W.A., Spera, F.J., 2001. Energy-constrained open-system magmatic processes II: application of energy-constrained assimilation-fractional crystallisation (EC-AFC) model to magmatic systems. *J. Petrol.* 42 (5), 1019–1041.
- Buck, W.R., 2004. Consequences of asthenospheric variability on continental rifting. In: Karner, G.D., et al. (Eds.), *Rheology and Deformation of the Lithosphere at Continental Margins*. Columbia University Press.
- Buck, W., 2006. The role of magma in the development of the Afro-Arabian Rift System. In: Yirgu, G., Ebinger, C.J., Maguire, P.K.H. (Eds.), *The Structure and Evolution of the East African Rift System in the Afar Volcanic Province*. In: *Spec. Publ. Geol. Soc. Lond.*, vol. 259, pp. 43–54.
- Buck, W.R., Lavier, L.L., Poliakov, A.N.B., 2005. Modes of faulting at mid-ocean ridges. *Nature* 434, 719–723.
- Cornwell, D.G., Mackenzie, G.D., England, R.W., Maguire, P.K.H., Asfaw, L.M., Oluma, B., 2006. Northern Main Ethiopian Rift crustal structure from new high-precision gravity data. In: Yirgu, G., Ebinger, C.J., Maguire, P.K.H. (Eds.), *The Afar Volcanic Province within the East African Rift System*. In: *Spec. Publ. Geol. Soc. Lond.*, vol. 259, pp. 307–321.
- Cox, K.G., Bell, J.D., Pankhurst, R.J., 1979. *The Interpretation of Igneous Rocks*. George Allen and Unwin.
- Craig, T.J., Jackson, J.A., Priestley, K., McKenzie, D., 2011. Earthquake distribution patterns in Africa: their relationship to variations in lithospheric and geological structure, and their rheological implications. *Geophys. J. Int.* 185 (1), 403–434.
- Daly, E., Keir, D., Ebinger, C.J., Stuart, G.W., Bastow, I.D., Ayele, A., 2008. Crustal tomographic imaging of a transitional continental rift: the Ethiopian rift. *Geophys. J. Int.* 172 (3), 1033–1048.
- Daniels, K., 2012. *Modelling magma transport: a study of dyke injection*. Ph.D. thesis. University of Bristol.
- Desissa, M., Johnson, N.E., Whaler, K.A., Hautot, S., Fisseha, S., Dawes, G.J.K., 2013. A mantle magma reservoir beneath an incipient mid-ocean ridge in Afar, Ethiopia. *Nat. Geosci.* 6, 861–865. <http://dx.doi.org/10.1038/ngeo1925>.
- Ebinger, C.J., Hayward, N.J., 1996. Soft plates and hot spots: Views from Afar. *J. Geophys. Res.* 101 (B10), 21859–21876.
- Ebinger, C.J., Casey, M., 2001. Continental breakup in magmatic provinces: An Ethiopian example. *Geology* 29, 527–530.
- Ebinger, C.J., van Wijk, J., Keir, D., 2013. The time scales of continental rifting: Implications for global processes. *Spec. Pap., Geol. Soc. Am.* 500. [http://dx.doi.org/10.1130/2013.2500\(11\)](http://dx.doi.org/10.1130/2013.2500(11)).
- Ferguson, D.J., Barnie, T.D., Pyle, D.M., Oppenheimer, C., Yirgu, G., Lewi, E., Kidane, T., Carn, S., Hamling, I., 2010. Recent rift-related volcanism in Afar, Ethiopia. *Earth Planet. Sci. Lett.* 292, 409–418.
- Ferguson, D.J., MacLennan, J., Bastow, I.D., Pyle, D.M., Jones, S.M., Keir, D., Blundy, J., Plank, T., Yirgu, G., 2013. Melting during late-stage rifting in Afar is hot and deep. *Nature* 499, 70–73. <http://dx.doi.org/10.1038/nature12292>.
- Ghiorso, M.S., Sack, R.O., 1995. Chemical mass transfer in magmatic processes. IV. A revised and internally consistent thermodynamic model for the interpolation and extrapolation of liquid-solid equilibria in magmatic systems at elevated temperatures and pressures. *Contrib. Mineral. Petrol.* 119, 197–212.
- Grandin, R., Jacques, E., Necessian, A., Ayele, A., Doubre, C., Socquet, A., Keir, D., Kassim, M., Lemarchand, A., King, G.C.P., 2011. Seismicity during lateral dike propagation: Insights from new data in the recent Manda Hararo–Dabbahu rifting episode (Afar, Ethiopia). *Geochem. Geophys. Geosyst.* 12 (4), Q0AB08.
- Gualda, G.A.R., Ghiorso, M.S., Lemons, R.V., Carley, T.L., 2012. Rhyolite-MELTS: A modified calibration of MELTS optimized for silica-rich, fluid-bearing magmatic systems. *J. Petrol.* 53 (5), 875–890.
- Hammond, J.O.S., Kendall, J.-M., Stuart, G.W., Keir, D., Ebinger, C., Ayele, A., Belachew, M., 2011. The nature of the crust beneath the Afar triple junction: Evidence from receiver functions. *Geochem. Geophys. Geosyst.* 12, Q12004.
- Hayward, N.J., Ebinger, C., 1996. Variations in the along-axis segmentation of the Afar Rift system. *Tectonophysics* 15 (2), 244–257.
- Hofstetter, R., Beyth, M., 2003. The Afar Depression: Interpretation of the 1960–2000 earthquakes. *Geophys. J. Int.* 155, 715–732.
- Jackson, J., 2002. Strength of the continental lithosphere: Time to abandon the jelly sandwich?. *GSA Today* 12, 4–10.
- Jaupart, C., Mareschal, J.-C., 2007. Heat flow and thermal structure of the lithosphere. In: Watts, A.B. (Ed.), *Crust and Lithosphere Dynamics*. In: *Treatise on Geophysics*, vol. 6, pp. 217–250.
- Jaupart, C., Mareschal, J.-C., 2011. *Heat Generation and Transport in the Earth*. Cambridge University Press.
- Keir, D., Hamling, I.J., Ayele, A., Calais, E., Ebinger, C., Wright, T.J., Jacques, E., Mohammed, K., Hammond, J.O.S., Belachew, M., Baker, E., Rowland, J.V., Lewi, E., Bennati, L., 2009. Evidence for focussed magmatic accretion at segment centres from lateral dike injections captured beneath the Red Sea Rift in Afar. *Geology* 37 (1), 59–62.
- Keir, D., Belachew, M., Ebinger, C., Kendall, J.-M., Hammond, J.O.S., Stuart, G.W., Ayele, A., Rowland, J.V., 2011a. Mapping the evolving strain field during continental breakup from crustal anisotropy in the Afar Depression. *Nat. Commun.* 2, 285. <http://dx.doi.org/10.1038/ncomms1287>.
- Keir, D., Pagli, C., Bastow, I., Ayele, A., 2011b. The magma-assisted removal of Arabia in Afar: Evidence from dike injection in the Ethiopian rift captured using InSAR and seismicity. *Tectonics* 30, TC2008. <http://dx.doi.org/10.1029/2010TC002785>.
- Keir, D., Bastow, I., Pagli, C., Chambers, E.L., 2013. Spatial and temporal constraints on mechanisms of continental breakup: evidence from Afar. *Tectonophysics*. <http://dx.doi.org/10.1016/j.tecto.2012.10.015>.
- Keranen, K., Klemperer, S.L., Gloaguen, R., Group, E.W., 2004. Three-dimensional seismic imaging of a protoridge axis in the main Ethiopian rift. *Geology* 32, 949–952.
- Kogan, L., Fisseha, S., Bendick, R., Reilinger, R., McClusky, S., King, R., Solomon, T., 2012. Lithospheric strength and strain localization in continental extension from observations of the East African Rift. *J. Geophys. Res.* 117, B03402.
- Laube, N., Springer, J., 1998. Crustal melting by ponding of mafic magmas: A numerical model. *J. Volcanol. Geotherm. Res.* 81, 19–35.
- Mackenzie, G.D., Thybo, H., Maguire, P.K.H., 2005. Crustal velocity structure across the Main Ethiopian Rift: Results from 2-dimensional wide-angle seismic modelling. *Geophys. J. Int.* 162, 994–1006.
- Maggi, A., Jackson, J., McKenzie, D., Priestley, K., 2000a. Earthquake focal depths, effective elastic thickness, and the strength of the continental lithosphere. *Geology* 28, 495–498.
- Maggi, A., Jackson, J., Priestley, K., Baker, C., 2000b. A reassessment of focal depth distributions in southern Iran, the Tien Shan and northern India: Do earthquakes really occur in the continental mantle?. *Geophys. J. Int.* 143, 629–661.
- Maguire, P.K.H., Keller, G.R., Klemperer, S.L., Mackenzie, G.D., Keranen, K., Harder, S., O'Reilly, B., Thybo, H., Asfaw, L., Khan, M.A., Amha, M., 2006. Crustal structure of the northern Main Ethiopian Rift from the EAGLE controlled source survey: a snapshot of incipient lithospheric break-up. In: Yirgu, G., Ebinger, C.J., Maguire,

- P.K.H. (Eds.), The Afar Volcanic Province within the East African Rift System. In: Spec. Publ. Geol. Soc. Lond., vol. 259, pp. 271–293.
- Makris, J., Ginzburg, A., 1987. The Afar Depression: transition between continental rifting and sea-floor spreading. *Tectonophysics* 141, 199–214.
- McClusky, S., Reilinger, R., Ogubazghi, G., Amleson, A., Healeb, B., Vernant, P., Sholan, J., Fisseha, S., Asfaw, L., Bendick, R., Kogan, L., 2010. *Geophys. Res. Lett.* 37, L05301.
- Michaut, C., Jaupart, C., 2006. Ultra-rapid formation of large volumes of evolved magma. *Earth Planet. Sci. Lett.* 250 (1–2), 38–52.
- Mohr, P.A., 1967. Major volcanotectonic lineament in the Ethiopian Rift System. *Nature* 213, 664–665.
- Nobile, A., Pagli, C., Keir, D., Wright, T.J., Ayele, A., Ruch, J., Acocella, V., 2012. Dike-fault interaction during the 2004 Dallol intrusion at the northern edge of the Erta Ale Ridge (Afar, Ethiopia). *Geophys. Res. Lett.* 39 (19), L19305.
- Pérez-Gussinyé, M., Metois, M., Fernández, M., Vergés, J., Fullea, J., Lowry, A.R., 2009. Effective elastic thickness of Africa and its relationship to other proxies for lithospheric structure and surface tectonics. *Earth Planet. Sci. Lett.* 287 (1), 152–167.
- Rivers, M.L., Carmichael, I.S.E., 1987. Ultrasonic studies of silicate melts. *J. Geophys. Res.* 92 (B9), 9247–9270.
- Rooney, T.O., Herzberg, C., Bastow, I.D., 2012. Elevated mantle temperature beneath East Africa. *Geology* 40 (1), 27–30, G32382. <http://dx.doi.org/10.1130/G32382.1>.
- Royden, L., Sclater, J.G., Von Herzen, R.P., 1980. Continental margin subsidence and heat flow: important parameters in formation of petroleum hydrocarbons. *Am. Assoc. Pet. Geol. Bull.* 64, 173–187.
- Solano, J.M.S., Jackson, M.D., Sparks, R.S.J., Blundy, J.D., Annen, C., 2012. Melt segregation in deep crustal hot zones: a mechanism for chemical differentiation, crustal assimilation and the formation of evolved magmas. *J. Petrol.* 53 (10), 1999–2026.
- Spera, F.J., 2000. Physical properties of magmas. In: Sigurdsson, H. (Ed.), *Encyclopedia of Volcanoes*. Academic Press, 1417 pp.
- Stern, C.R., Wyllie, P.J., 1973. Water-saturated and undersaturated melting relations of a granite to 35 kilobars. *Earth Planet. Sci. Lett.* 18, 163–167.
- Tesfaye, S., Harding, D.J., Kusky, T.M., 2003. Early continental breakup boundary and migration of the Afar triple junction, Ethiopia. *GSA Bull.* 115 (9), 1053–1067.
- Thybo, H., Nielsen, C.A., 2009. Magma compensated crustal thinning in continental rift zones. *Nature* 457, 873–876. <http://dx.doi.org/10.1038/nature07688>.
- Tiberi, C., Ebinger, C., Ballu, V., Stuart, G.W., Oluma, B., 2005. Inverse models of gravity data from the Red Sea-Aden-East African rifts triple junction zone. *Geophys. J. Int.* 163 (2), 775–787.
- Turcotte, D.L., Schubert, G., 2002. *Geodynamics*. Cambridge University Press, 456 pp.
- Whaler, K.A., Hautot, S., 2006. The electrical resistivity structure of the crust beneath the northern Main Ethiopian Rift. In: Yirgu, G., Ebinger, C.J., Maguire, P.K.H. (Eds.), *The Afar Volcanic Province within the East African Rift System*. In: Spec. Publ. Geol. Soc. Lond., vol. 259, pp. 293–305.
- White, R.S., Smith, L.K., Roberts, A.W., Christie, P.A.F., Kuszniir, N.J., the rest of the iSIMM Team, 2008. Lower crustal intrusion on the North Atlantic continental margin. *Nature* 452, 460–464. <http://dx.doi.org/10.1038/nature06687>.
- Witham, F., 2008. The degassing of basaltic magma chambers. Ph.D. thesis. University of Bristol.
- Wolfenden, E., Ebinger, C., Yirgu, G., Renne, P., Kelley, S.P., 2005. Evolution of the southern Red Sea rift: birth of a magmatic margin. *Geol. Soc. Am. Bull.* 117, 846–864.
- Wright, T.J., Ebinger, C., Biggs, J., Ayele, A., Yirgu, G., Keir, D., Stork, A., 2006. Magma-maintained rift segmentation at continental rupture in the 2005 Afar dyking episode. *Nature* 42, 291–294.
- Yoder, H.S., Tilley, C.E., 1962. Origin of basalt magmas – an experimental study of natural and synthetic rock systems. *J. Petrol.* 3 (3), 342–532.

### Further reading

Carslaw, H.S., Jaeger, J.C., 1950. *Conduction of Heat in Solids*. Oxford University Press.